NUMERICAL SIMULATION OF THE HYLON (HYDROGEN LOW NOX) BURNER USING AN AUTONOMOUS MESHING APPROACH WITH DETAILED CHEMISTRY

Suresh Nambully
CONVERGENT Science GmbH Linz, Austria

Shuaishuai Liu
CONVERGENT Science Inc., USA

Eric Pomraning
CONVERGENT Science Inc., USA

Daniel Lee
CONVERGENT Science Inc., USA

Tristan Burton
CONVERGENT Science Inc., USA

Yajuvendra Shekhawat
CONVERGENT Science India Pune, India

Kelly Senecal
CONVERGENT Science Inc., USA

Matteo Fiaschi
CONVERGENT Science GmbH Linz, Austria

Mathias Vångö
CONVERGENT Science GmbH Linz, Austria

Abstract

A sustainable future of power and aviation puts more and more demand on the usage of carbon-neutral fuels to reduce emissions. To that end, hydrogen possesses several desirable characteristics and is thus a strong candidate. However, burning hydrogen comes with other challenges, primarily related to flame stabilization and relatively large NO_x emissions. Thus, to enable the usage of hydrogen as a fuel in these industries, combustors must be designed to minimize NO_x emissions and flashback risk.

Computational Fluid Dynamics (CFD) has proven to be a great tool to model the combustors to achieve these targets. In this work, we employ the CONVERGE CFD code, using a detailed chemistry and Adaptive Mesh Refinement (AMR) approach to model the Hydrogen Low NO_x (HYLON) [1] burner by IMFT, Toulouse. Here, the numerically obtained NO_x production and velocity distribution for two types of flames; attach and lifted, are compared with the experimental data.

Introduction

Decarbonization of the power and aviation industries has led to the exploration of hydrogen as an alternative fuel, due to its lack of hydro-carbons and consequently CO and CO_2 emissions. However, hydrogen is highly reactive and burns at comparatively higher temperatures than conventional fuels. This leads to challenges related to flame stabilization, such as flashback and NO_x emissions which must be considered in the burner design.

To study these challenges in detail, IMFT, Toulouse developed the dual-swirl HYLON [1] burner, where experiments were conducted on both lifted and attached flames. In these tests it was observed that the lifted flame produced significantly lower NO_x than the attached flame. Additionally, these tests serve as valuable validation data for numerical models.

By utilizing CFD to study burners numerically, a much greater insight can be obtained and aid the development of a new generation of combustors. However, the hydrogen combustion process poses numerous additional challenges to the numerical model. For one, hydrogen has a lower Schmidt number than hydro-carbon fuels which leads to faster mixing with the oxidizer. Furthermore, the chemical kinetics plays a key role in reliably predicting flame positions, flame shapes and emissions.

Aniello et. al [2] simulated the HYLON [1] burner using the thickened flame combustion model, where the authors proposed a unique flame stabilization mechanism based on the mixing and the velocity field. In that work, they also highlight the importance of thermo-diffusive effects on the flame stabilization. However, only the lifted flame was studied.

In this work, we use the CFD code CONVERGE CFD [3] to simulate both the attached and lifted configurations of the HYLON [1] burner, using a Large Eddy Simulation (LES) approach together with AMR and a detailed chemistry combustion model. The numerical model is validated by comparing to the experimental measurements.

Test case description

The HYLON [1] burner has two separate inlets for air and hydrogen to reduce the flashback risks. Both the streams have separate swirlers; a radial swirler for the air and an axial swirler for the hydrogen, as illustrated in Figure 1. The swirl number for air is 6.5, whereas the one for hydrogen is 0.9.

Both the fuel and oxidizer streams enter the domain with 298 K temperature and start to mix just before the exit of the burner. Based on the flow rates, the two different flame configurations can be observed. The flow rates of both streams are given in Table 1 for both the attached (case A) and lifted flame (case L). Both cases have an equivalence ratio of 0.4.

Furthermore, PIV measurements for the velocity distribution, flame images using OH* chemiluminescence and NO_x measurements are available to validate the simulation results.

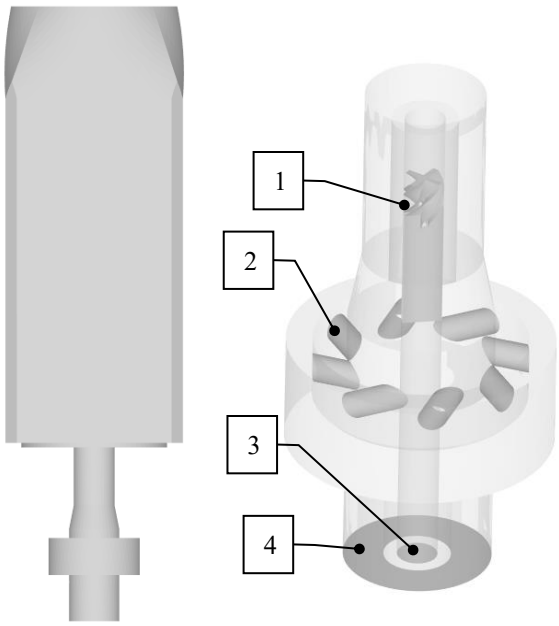

Figure 1: HYLON burner geometry [1] (1 – fuel swirler, 2 – air swirler, 3 – fuel inlet, 4 – air inlet).

Flame Type	Fuel Flow rate [g/s]	Air Flow rate [g/s]
Attached (case A)	0.032	2.41
Lifted (case L)	0.08	6.03

Table 1: Fuel and air flow rate for the attached and lifted flame configurations.

Simulation setup

The CFD simulations are performed using the CONVERGE CFD [3] and the physical models used are described in this section.

Turbulence model

A two-equation LES model is used which was developed to be consistent with an Adaptive Mesh Refinement (AMR) algorithm. In an LES simulation, it is typical to assume that the filter size is equal to the grid size. This presents a challenge in an LES simulation with AMR as the grid size may change every time-step. Specifically, when a cell is embedded due to AMR, it is incorrect to assume that the filter size is immediately equal to the grid size as it will take time for the enhanced resolution to resolve more scales. Clearly, there is a need to calculate a time evolving filter size. For example, consider a zero-equation LES model such as the Smagorinsky model. The sub-grid scale viscosity for the Smagorinsky model is proportional to the filter size squared. Now consider an AMR embedding event where a cell size is divided in half. If the filter size is assumed to be equal to the grid size and a cell is embedded due to AMR, the sub-grid scale viscosity would be reduced by a factor of four even though no additional scales have been resolved immediately during the embedding process. It takes time to resolve the scales that will develop from the new finer grid. To solve this problem, a two-equation dynamic structure LES model is used in this work [3, 4].

To show the complete model, we start with the LES transport equation for momentum given by

$$\frac{\partial \bar{\rho}\tilde{u}_i}{\partial t} + \frac{\partial \bar{\rho}\tilde{u}_i\tilde{u}_j}{\partial x_j} = -\frac{\partial \bar{P}}{\partial x_i} + \frac{\partial \overline{\sigma_{ij}}}{\partial x_j} - \frac{\partial \tau_{ij}}{\partial x_j}$$

Where the sub-grid stress tensor is given by

$$\tau_{ij} = \bar{\rho}\left(\widetilde{u_i u_j} - \tilde{u}_i\tilde{u}_j\right)$$

The sub-grid stress tensor is modeled by

$$\tau_{ij} = 2\bar{\rho}kc_{ij}$$

where the sub-grid kinetic energy is given by

$$k = \frac{1}{2}\left(\widetilde{u_i u_j} - \tilde{u}_i\tilde{u}_j\right)$$

and the dynamic structure coefficient tensor is given by

$$c_{ij} = \frac{L_{ij}}{L_{kk}}$$

The Leonard stress tensor is given by

$$L_{ij} = \widehat{\tilde{u}_i\tilde{u}_j} - \hat{\tilde{u}}_i\,\hat{\tilde{u}}_j$$

where the $\widehat{\ }$ indicates a test filter operation. In this case, the test filter is twice the size of the grid. Notice that the model for the sub-grid scale tensor does not use a sub-grid scale viscosity formulation for closure.

The two-equation dynamic structure model is derived from the one-equation dynamic structure model with an additional equation for the sub-grid scale dissipation. The two-equation dynamic structure model uses two transport equations. One transport equation for sub-grid kinetic energy k and one for the sub-grid dissipation ε:

$$\frac{\partial \bar{\rho}k}{\partial t} + \frac{\partial \bar{\rho}\tilde{u}_i k}{\partial x_i} = -\tau_{ij}\frac{\partial \tilde{u}_i}{\partial x_j} - \varepsilon + \frac{\partial}{\partial x_i}\left(\frac{\mu_{\text{sgs}}}{\sigma_k}\frac{\partial k}{\partial x_i}\right)$$

where sub-grid dissipation tranport equation is given by

$$\frac{\partial \bar{\rho}\varepsilon}{\partial t} + \frac{\partial \bar{\rho}\tilde{u}_i\varepsilon}{\partial x_i} = \left(\frac{3C_\varepsilon\bar{\rho}\varepsilon}{2k}\right)P - \frac{3\bar{\rho}\varepsilon^2}{2k} + \frac{\partial}{\partial x_i}\left(\frac{\mu_{sgs}}{\sigma_\varepsilon}\frac{\partial \varepsilon}{\partial x_i}\right) + \frac{\bar{\rho}\varepsilon}{l_f}\left(\frac{\Delta_f - \Delta_g}{\tau}\right)$$

here P is the sub-grid production, Δ_f is the local filter size, andτ is the time-scale over which Δ_f relaxes to the local grid filter size Δ_g. The local filter size is defined to be

$$\Delta_f = \frac{C_\varepsilon k^{3/2}}{\varepsilon}$$

The time scale is given by

$$\tau = \frac{C_z k}{\varepsilon}$$

With the two equation formulation the local filter size will not immediately become the local grid size, and it will evolve in time. The sub-grid scale viscosity is defined as:

$$\mu_{\text{sgs}} = C_k \bar{\rho} k^{1/2} \Delta_f = C_k C_\varepsilon \bar{\rho} \frac{k^2}{\varepsilon}$$

where C_ε and C_k are model constants. Note that unlike the momentum equation, the dynamic structure model uses the sub-grid scale viscosity to close the energy transport equation and the species transport equations.

The two-equation dynamic structure model is recommended for use with simulations using Adaptive Mesh Refinement (AMR).

Combustion model

Many turbulent combustion models have been developed in the past decades, including probability density function (PDF)-based models, flamelet-based models (FGM), finite-rate chemistry models, etc.

Among these combustion models, the finite-rate chemistry model shows many advantages. It can be used with both RANS and LES. For non-premixed flames, the finite-rate chemistry model can be understood as a single-delta PDF model, while for premixed flames it can be considered as a thickened flame-type model. The finite-rate chemistry model does not assume the species compositions are confined to a low-dimensional manifold, which ensures broader applicability of this model. A detailed chemistry mechanism may contain hundreds of species. Such large mechanisms may be essential for chemical-kinetics-control processes, e.g., ignition and emission prediction [5]. It is straightforward to couple a finite chemistry model with a more complicated multicomponent diffusion model which is important for H_2 combustion.

For current work, the finite-rate chemistry model is fully-coupled with all the species transport equations. To speed up the chemistry calculation, the adaptive-zone technique which groups cells with similar conditions based on temperature and equivalence ratio is used. A complete description of adaptive zone technique and combustion predictions with and without the multi-zone model, can be found [6].

Chemical mechanism

The H_2 mechanism is extracted from a comprehensive chemical mechanism C3MechV3.5 which has been validated using a wide range of experimental results for pure hydrogen and hydrogen blends with different fuels. These validations target different data sets which include ignition delay, laminar flame speed, and species profiles as a function of time. [7].

To reduce the computational time, the original extracted H_2 mechanism is reduced with an enhancement of the Direct Relation Graph (DRG) technique called Parallel DRG-with Error Propagation and Sensitivity Analysis (PDRGEPSA) [6]. The reduction was performed for pressures from 1 to 60 atm, equivalence ratios from 0.5 to 2, and an initial temperature range of 600-1500 K using ignition delay, laminar flame speed and the NOX level as targets.

The final reduced H_2 mechanism contains 20 species, 100 reactions while the original mechanism contains 34 species and 236 reactions. Figure 2 shows the results comparison between the original and reduced mechanism.

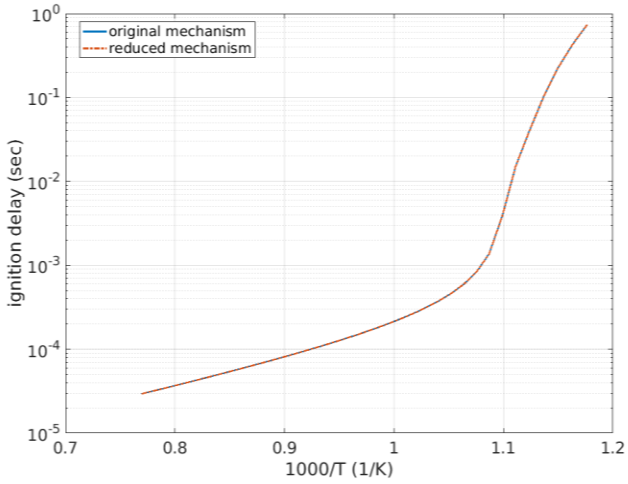

(a) H_2 ignition time of equivalence ratio 1.0, pressure 1 bar

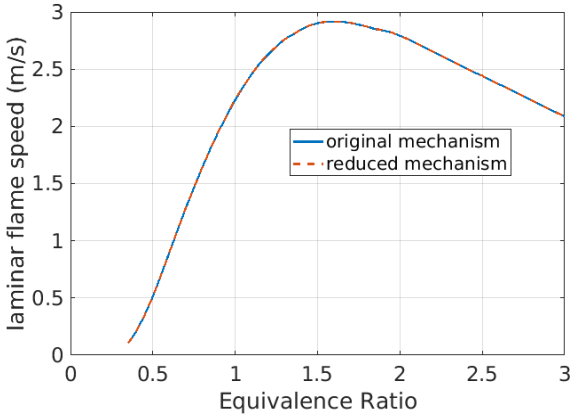

fd

(b) H_2 flame speed at unburned temperature 300K, pressure 1 bar

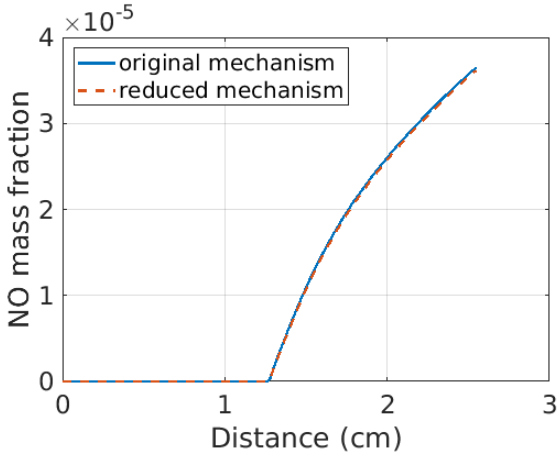

(c) NO 1D profile at equivalence ratio 0.8, unburned temperature 300K, pressure 1 bar

Figure 2: Results comparison between the original and the reduced mechanism.

Adaptive Mesh Refinement

One of the major pre-processing steps in CFD simulations is the mesh generation. In CONVERGE, the mesh is generated automatically during runtime using a modified cartesian cut-cell approach, which enables the use of AMR as the primary method for mesh refinement.

AMR is a mesh refinement method, used to dynamically refine or coarsen the mesh based on normalized second derivatives of local flow quantities. In this work, AMR was applied based on velocity as well as H_2 and OH concentrations. A snapshot of the mesh is depicted in Figure 3 for the attached flame, together with the Length Scale Resolution (LSR) parameter used to evaluate the turbulence resolution [8].

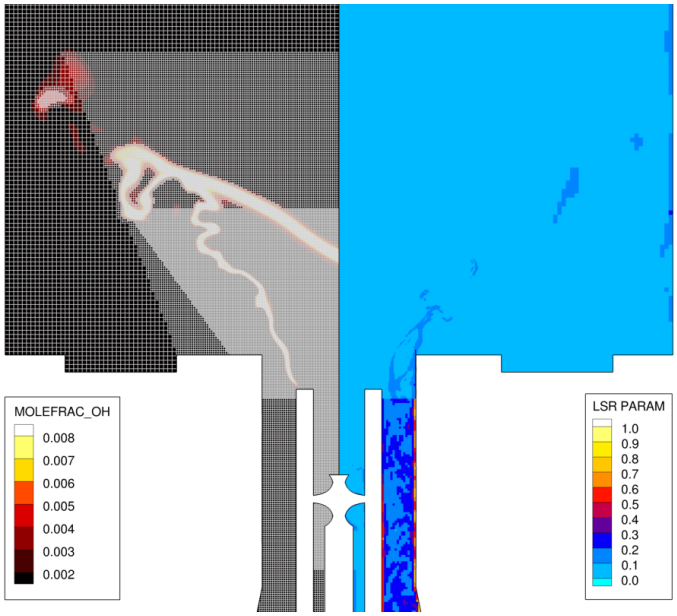

Figure 3: Visualization of the mesh and OH mole fraction (left), as well as the LSR parameter (right).

The minimum cell size used in the simulations was 0.125 mm, which was chosen to be smaller than the expected minimum turbulent flame thickness. The turbulent flame thickness was estimated based on the laminar flame thickness, calculated from 1D flame calculations, and the equivalence ratio. The maximum cell count used was approximately 30 million. Such a fine mesh is required to properly resolve the flame front, as the flame is predominantly diffusive and hence the Thickened Flame Model (TFM) is not very applicable. To check the flame type, a normalized flame index ξ has been evaluated for both flames [9]. Figures 4 and 5 show that flame A is completely diffusive and flame L is partially premixed.

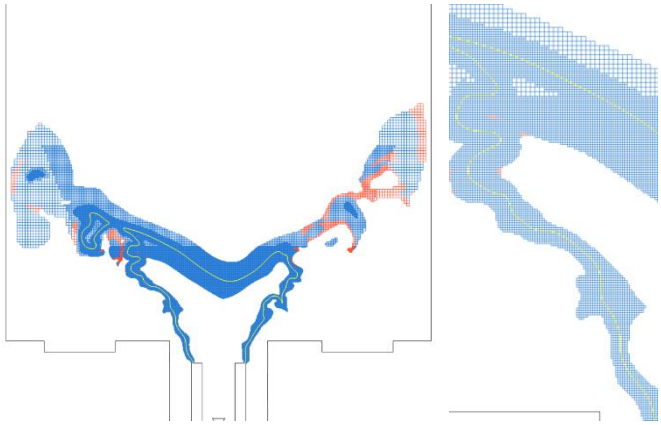

Figure 4: Case A, isolated zone of OH mole fractions greater than 1e-04. The yellow line indicates the stoichiometric ratio. Blue indicates a diffusive flame and red a premixed one.

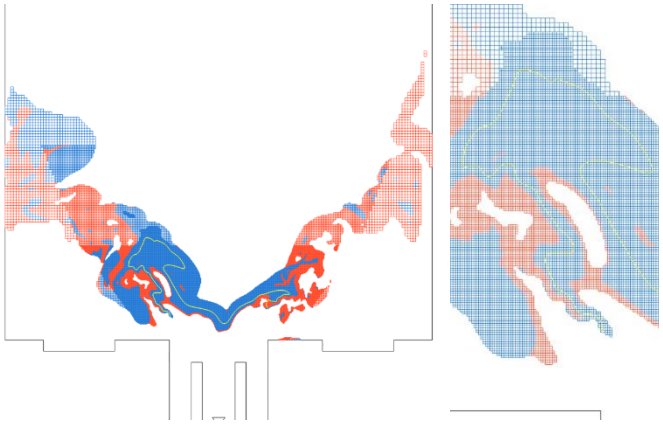

Figure 5: Case L, isolated zone of OH mole fractions greater than 1e-04. The yellow line indicates the stoichiometric ratio. Blue indicates a diffusive flame and red a premixed one.

CFD results

In order to compare with the experiments, we ran case A and L both in non-reacting and reacting conditions. For the non-

reacting cases, time-averaged results are compared with the measured velocity field and hydrogen concentration distribution. Whereas in the reacting cases, the time-averaged velocity field, as well as a few global quantities such as NO_x emissions, outflow temperature and pressure drop are compared.

Non-reacting flow

The results of the non-reacting case A and L have been sampled over a physical time of 40 ms and 33 ms respectively. In both cases, enough time was simulated before starting collecting the statistics to ensure no deleterious effects of the initial conditions.

Velocity field

The velocity field comparison between the CFD simulations and the experiments shown in Figures 6 and 7 indicates that both the averaged axial and radial velocity components are well captured. Evidently the simulations are capable of accurately reproducing the recirculation zone and the flow rotation imposed by the swirlers. Furthermore, the velocity fluctuations in both the axial and radial directions are in line with the experiments.

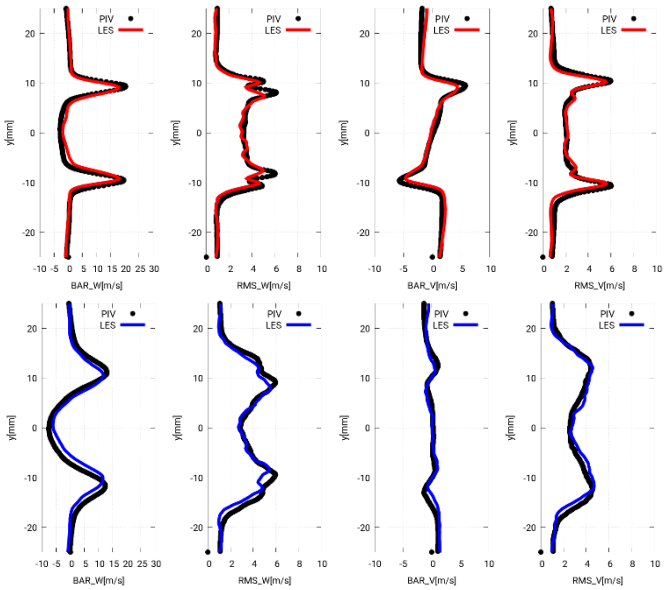

Figure 6: Non-reacting case A, average and RMS of axial velocity (W) and radial velocity (V) sampled at z=5 mm (red) and z=15 mm (blue) compared with PIV measurements (black).

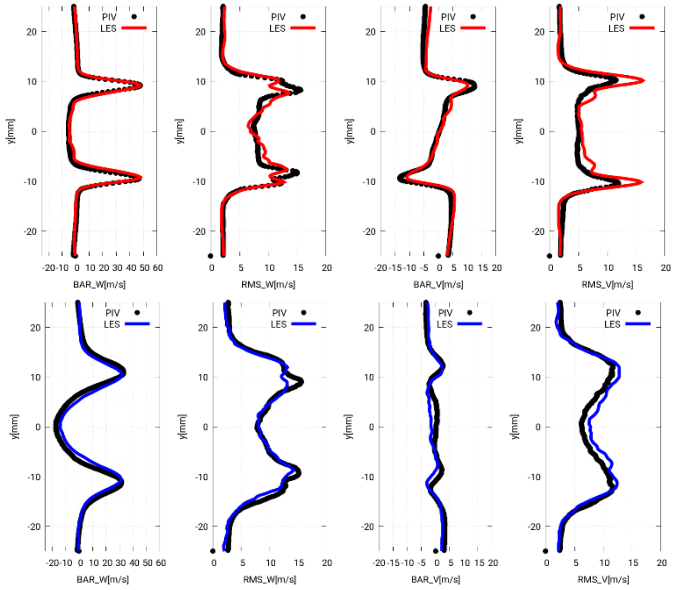

Figure 7: Non-reacting case L, average and RMS of axial velocity (W) and radial velocity (V) sampled at z=5 mm (red) and z=15 mm (blue) compared with PIV measurements (black).

Hydrogen distribution

Figure 8 depicts the comparison between the averaged hydrogen mole fraction and the measurements at various heights. The simulations are matching qualitatively but not quantitatively close to the pipe exit (z=1 mm), however the agreement improves further downstream.

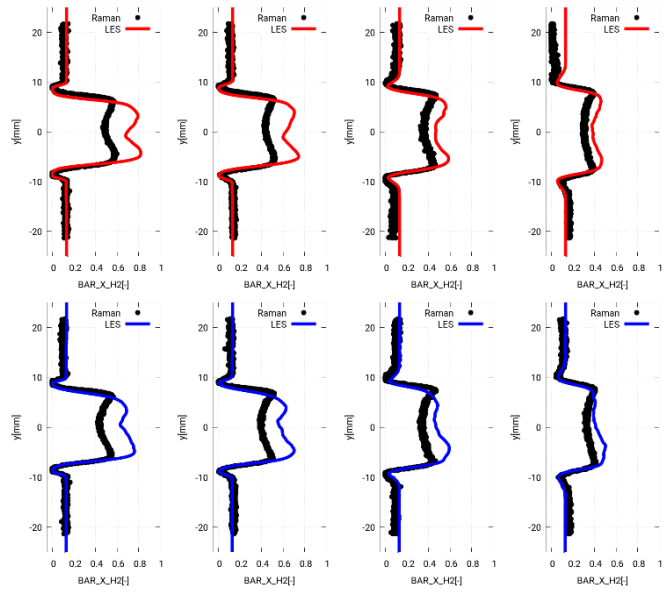

Figure 8: Averaged hydrogen mole fraction for the non-reacting case A (red) and case L (blue) compared measurements (black) at various heights. From left to right at: z=1 mm, z=2 mm, z=4 mm, z=6 mm.

Reacting flow

The results of the reacting case A and L have been sampled over a physical time of 16.5 ms and 15 ms respectively.

Velocity field

Like the non-reacting cases, Figures 9 and 10 show the axial and radial velocity profile at various distances downstream from the nozzle exit. The simulations are capable of satisfactorily predicting the axial and radial velocity profile.

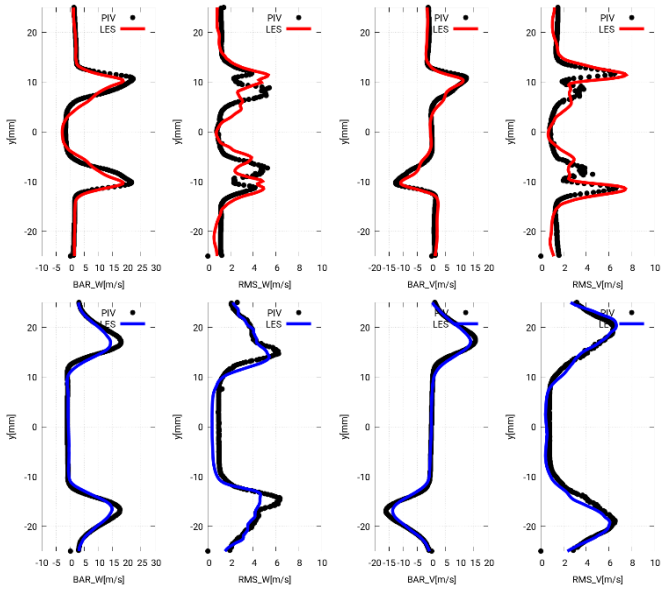

Figure 9: Reacting case A, average and RMS of axial velocity (W) and radial velocity (V) sampled at z=5 mm (red) and z=15 mm (blue) compared with PIV acquisitions (black).

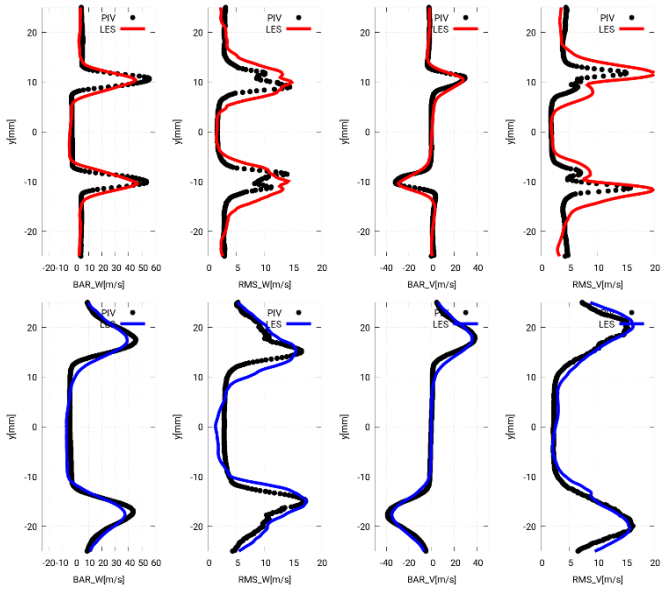

Figure 10: Reacting case L, average and RMS of axial velocity (*W*) and radial velocity (*V*) sampled at *z*=5 mm red) and *z*=15 mm blue) compared with PIV acquisitions (black).

Global quantities

The simulated pressure drops from the hydrogen and air supply streams compared to ambient were also compared and are reported in Table 2. In general, good agreements for the air stream were found in both cases, whereas underpredictions were observed for the hydrogen. However, there are some uncertainties to the hydrogen comparison, as the measurement point was located further upstream than what was covered by the simulation domain, as visualized in Figure 11.

Case	ΔP_{air} (Pa)	ΔP_{H2} (Pa)
$A_{Exp.}$	918	165
$A_{Sim.}$	919 (+0.1%)	144* (-12.2%)
$L_{Exp.}$	5752	821
$L_{Sim.}$	5847 (+1.6%)	642* (-21.7%)

Table 2: Comparison of the pressure drops from the air and hydrogen supply streams to ambient, between the simulations and experiments. The symbol * indicates that there is a mismatch in monitor location.

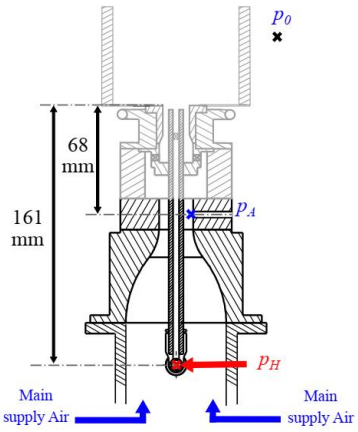

Figure 11: Scheme of the HYLON burner with locations of pressure measurement points.

The burner outflow temperature and NO_x emissions are reported in Table 3. In both cases, there is a trend of underpredicting the temperature as well as the NO_x emissions. One reason for this trend could be due to the combustion chamber wall boundary conditions applied. The values used are from thermocouple readings immersed in the solid walls, rather than the surface itself. Typically, the surface temperature is greater than the thermocouple reading, and could cause the underestimation of temperature and consequently the NO_x emissions observed.

Case	T_{out} (K)	NO (ppm)	NO_2 (ppm)
$A_{Exp.}$	1160.4 (exp. avg.)	12.1	1.1
A_{LES}	1044.35 (-10.0%)	10.48	1.11
$L_{Exp.}$	1372.7 (exp. avg.)	6.2	0.7
L_{LES}	1136.57 (-17.2%)	3.69	0.294

Table 3: Comparison of outflow temperature and NO_x emissions between the simulations and experiments.

Heat release rate

Figures 12 and 13 depict the comparison of the normalized heat release rate between the simulations (right) and experiments (left) for the two cases. A good agreement was obtained regarding both flame position and shape.

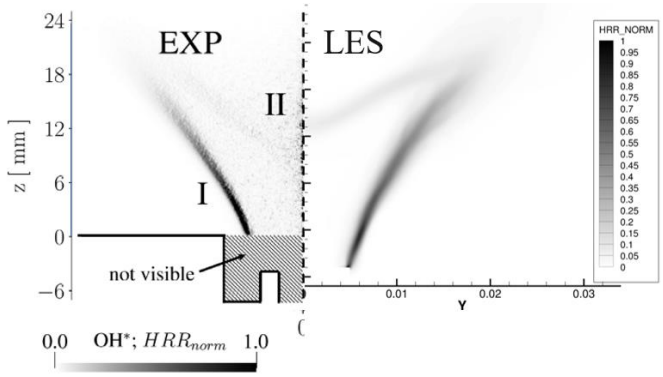

Figure 12: Flame A, comparison of the measured Abel-deconvoluted OH* chemilumineschence (left) and simulated normalized heat release rate (right).

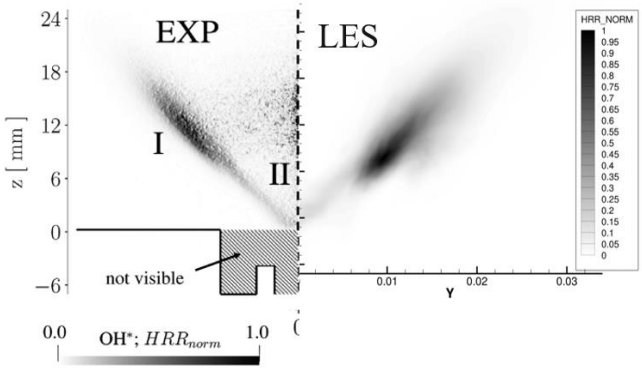

Figure 13: Flame L, comparison of the measured Abel-deconvoluted OH* chemilumineschence (left) and simulated normalized heat release rate (right).

NO_x emissions

Figures 14 and 15 show the NO and NO_2 production and consumption in the zone where OH is present, colored by temperature. We can observe a linear correlation between the production and consumption of NO and NO_2, and that at high temperatures, only the production of NO is present. Additionally, the plot is more scattered in case L, which agrees with the observations from Figure 5 that case L experiences a broader range of conditions.

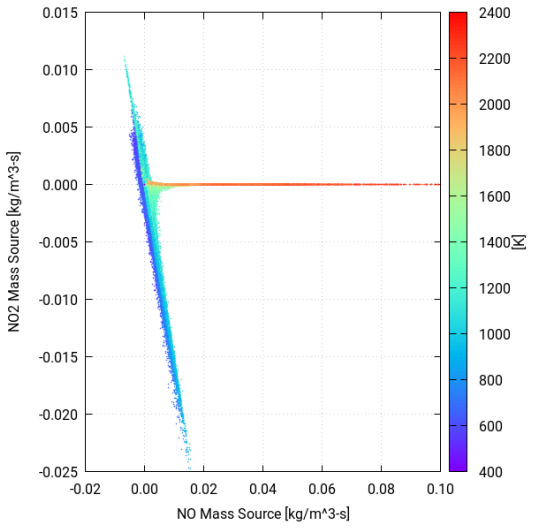

Figure 14: Case A, correlation of NO-NO_2 production and consumption in the zone where OH mole fraction is greater than 1e-04. The points are colored by temperature.

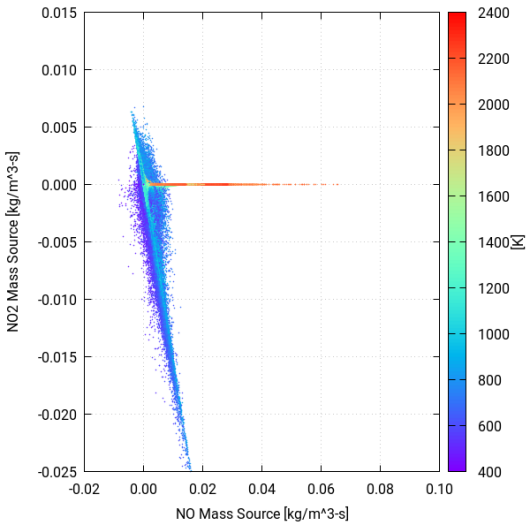

Figure 15: Case L, correlation of NO-NO_2 production and consumption in the zone where OH mole fraction is greater than 1e-04. The points are colored by temperature.

Conclusion

In this work, we presented a numerical approach using an autonomous mesh, two-equation LES together with detailed chemistry to simulate the Hydrogen Low NO_x (HYLON) burner. The numerical model was validated against the measurements of

the dual-swirl HYLON burner by IMFT, Toulouse [1] for two types of flames; attached and lifted.

More specifically, we compared the velocity distributions at various planes downstream of the nozzle in both non-reacting and reacting configurations. Additionally, in the non-reacting cases, the hydrogen concentration was also evaluated at those planes. Furthermore, in the reacting cases, the flame shape and position were also studied, together with NO_x emissions and pressure drop as well as outflow temperature.

In general, the model did well in reproducing the measured experimental results with a satisfactory level of accuracy. This validation study shows that the selected numerical model can serve as a valuable tool for the design of future hydrogen combustors.

References

[1] Sylvain Marragou, Hervé Magnes, Andrea Aniello, Laurent Selle, Thierry Poinsot, et al.. Experimental analysis and theoretical lift-off criterion for H2/air flames stabilized on adual swirl injector. Proceedings of the Combustion Institute, In press, ff10.1016/j.proci.2022.07.255ff. ffhal-03880308.

[2] A. Aniello, D. Laera, L. Berger, A. Attilik AND T. Poinsot, 2022, “Introducing thermodiffusive effects in large-eddy simulation of turbulent combustion for lean hydrogen-air flames”, Center for Turbulence Research, Proceedings of the Summer Program 2022.

[3] Richards, K. J., Senecal, P. K., and Pomraning, E., 2023, “CONVERGE (Version 3.1) Manual,” Convergent Science, Inc., Madison, WI..

[4] Pomraning, E., Rutland, C. J., 2002, “Dynamic One-Equation Nonviscosity Large-Eddy Simulation Model,” AIAA Journal, 40(4), pp. 689-701

[5] Liu, Shuaishuai, et al. "Towards Accurate Temperature and Species Mass Fraction Predictions for Sandia Flame-D using Detailed Chemistry and Adaptive Mesh Refinement." *2018 AIAA Aerospace Sciences Meeting*. 2018.

[6] Raju, Mandhapati, et al. "A reduced diesel surrogate mechanism for compression ignition engine applications." Internal Combustion Engine Division Fall Technical Conference. Vol. 55096. American Society of Mechanical Engineers, 2012

[7] Shijun Dong, Scott W. Wagnon, Luna Pratali Maffei, Goutham Kukkadapu, Andrea Nobili, Qian Mao, Matteo Pelucchi, Liming Cai, Kuiwen Zhang, Mandhapati Raju, Tanusree Chatterjee, William J. Pitz, Tiziano Faravelli, Heinz Pitsch, Peter Kelly Senecal, Henry J. Curran, A new detailed kinetic model for surrogate fuels: C3MechV3.3, Applications in Energy and Combustion Science, Volume 9, 2022, 100043, ISSN 2666-352X

[8] Piscaglia, Federico, Andrea Montorfano, and Angelo Onorati. "Towards the LES simulation of IC engines with parallel topologically changing meshes." *SAE International Journal of Engines* 6.2 (2013): 926-940.

[9] Rosenberg, David A., Patton M. Allison, and James F.Driscoll. "Flame index measurements to assess partially-premixed flame models." *8th US National Combustion Meeting, Park City, UT*. 2013.